nature medicine

Supplementary information

https://doi.org/10.1038/s41591-024-03073-9

Spatial multiomic landscape of the human placenta at molecular resolution

In the format provided by the authors and unedited

Supplementary Information

Supplementary Fig. 1

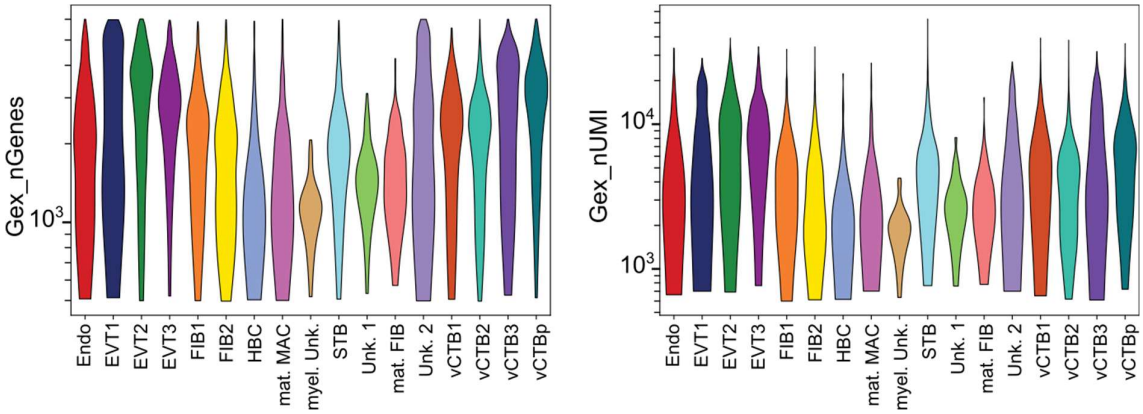

Supplementary Fig. 1, related to Fig. 1

Violin plots showcasing the distribution of gene expression metrics, separated by clusters. The plot's left side represents the distribution of number of genes detected (Gex_nGenes) per cell across clusters, whereas the right side shows the distribution of the number of unique molecular identifiers (Gex_nUMI) per cell for each cluster. Further QC metrics can be found in Supplementary Table 1.

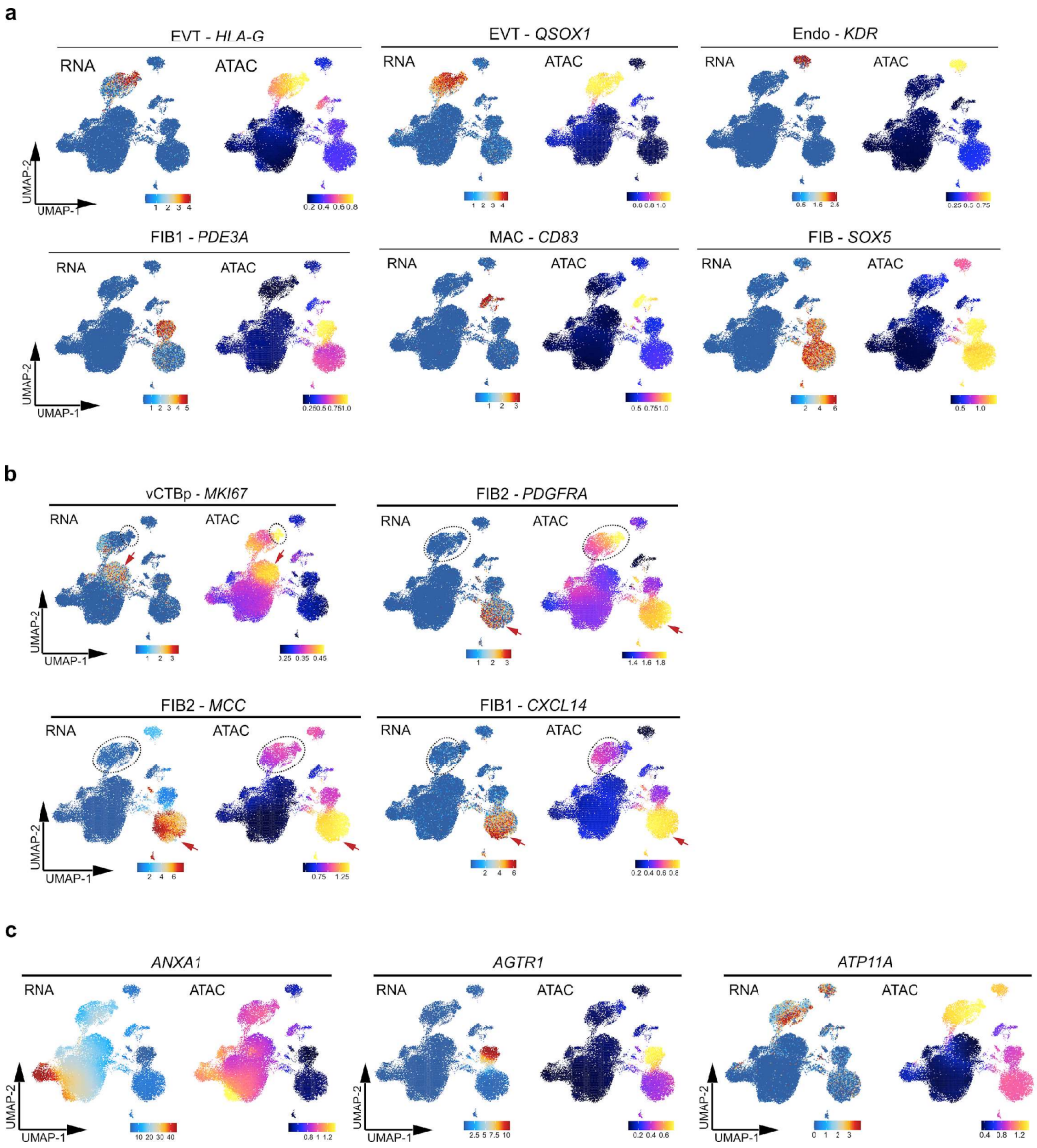

Supplementary Fig. 2, related to Extended Data Fig. 2

a, Additional visual comparison of gene expression (RNA) and gene activity score (ATAC) UMAP plots for selected marker genes including *HLA-G, QSOX1, KDR, PDE3A, CD83,* and *SOX5* to support the use of gene activity scores.

b, UMAP representation of extra chromatin accessibility of *MKI67, PDGFRA, MCC,* and *CXCL14* not reflected by gene expression. Arrows point to overlapping gene expression (RNA) and chromatin accessibility (ATAC). Stippled lines encircle cell clusters with extra chromatin accessibility.

c, UMAP representation of novel cell type-specific genes identified by snATAC-seq analysis, including *ANXA1* (vCTB3, STB), *AGTR1* (FIB1), and *ATP11A* (EVT, Endo).

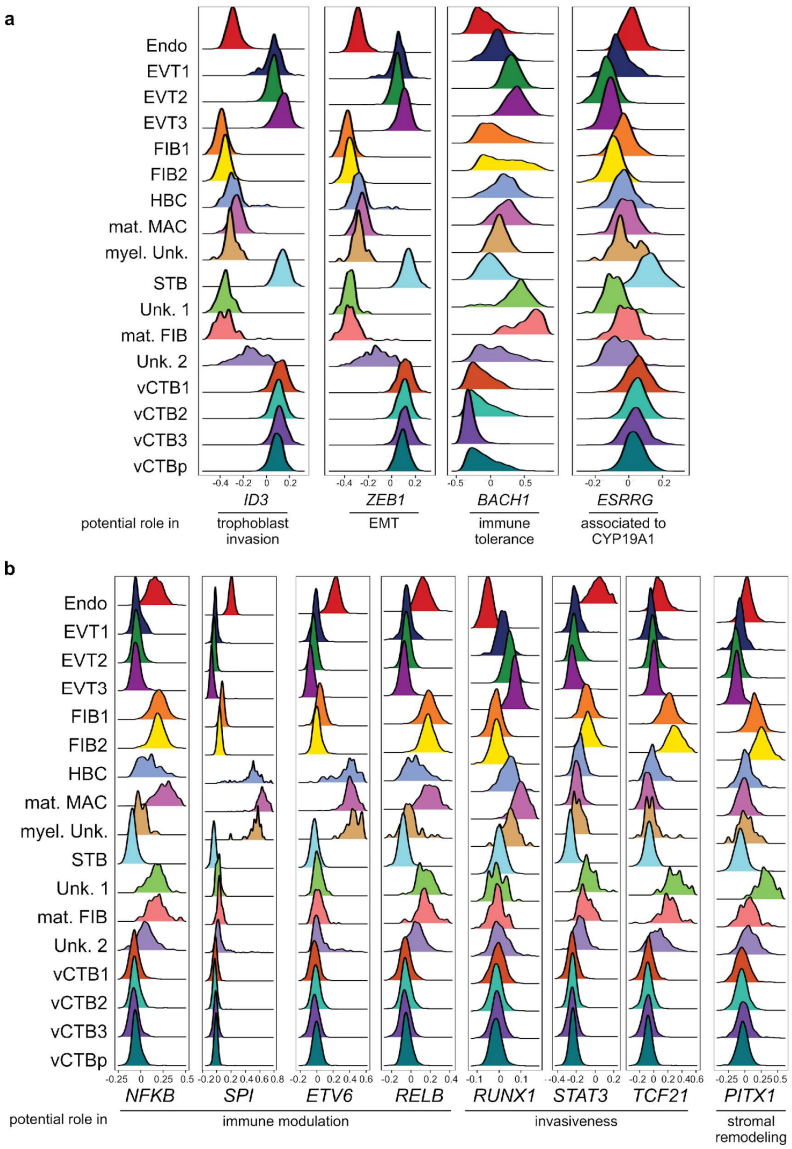

Supplementary Fig. 3, related to Fig. 2 and Extended Data Fig. 2

a, Motif track visualization showing regions of open chromatin for *ID3* (trophoblast invasion), *ZEB1* (EMT), *BACH1* (immune tolerance), and *ESRRG* (associated with CYP19A1, unclear role in trophoblast function). *BACH1* and *ESRRG* were originally found during intercluster motif enrichments and reinforced with ChromVAR and positive TF regulator analysis, whereas *ID3* and *ZEB1* were newly identified by ChromVAR and positive TF regulator analysis.

b, Plotted tracks showing regions of open chromatin in identified positive TF regulators with potential roles in immunomodulation (*NFKB1*[1], *SPI1*[2], *ETV6*[3], *RELB*[4,5]), invasiveness (*RUNX1*, *STAT3*[6], *TCF21*[7]), and remodeling of the placental stroma (*PITX1*[8]).

Supplementary Fig. 4

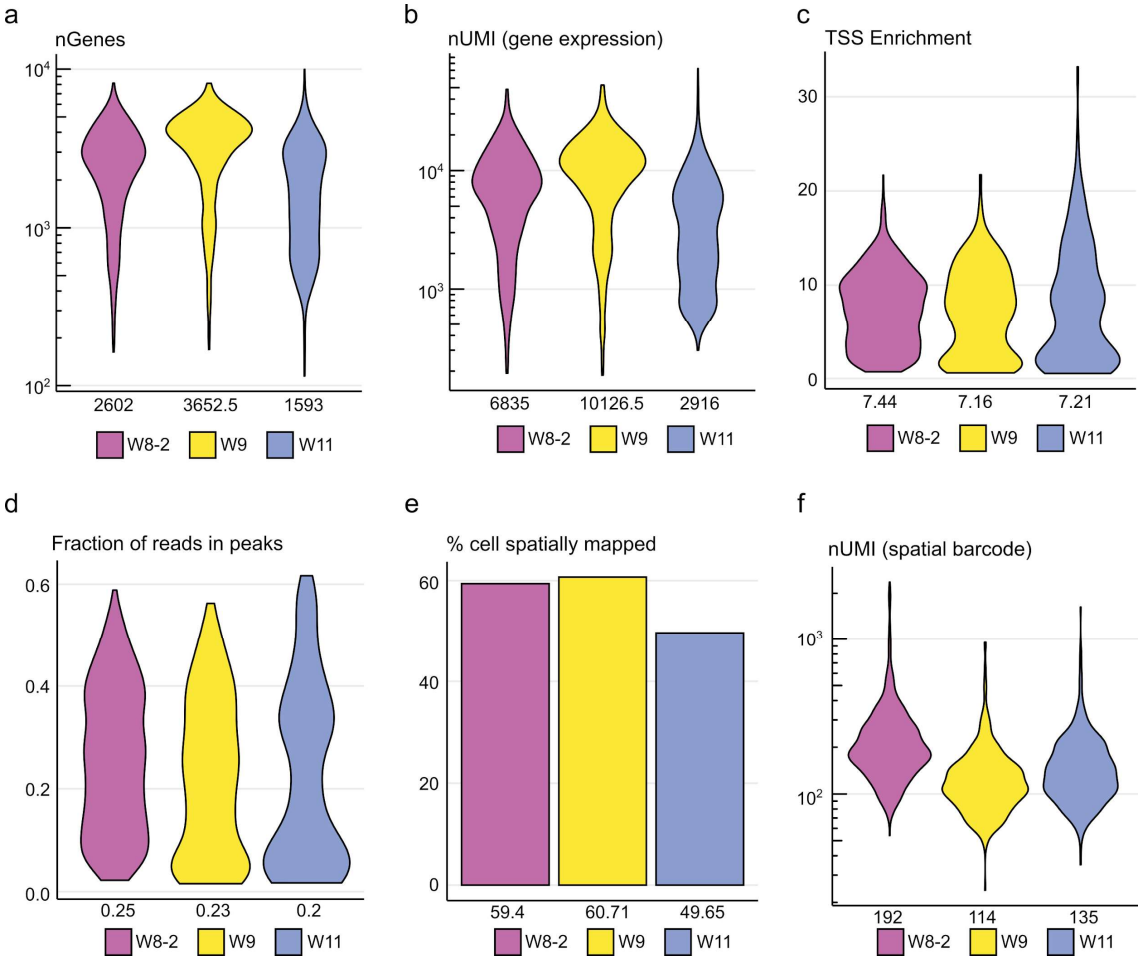

Supplementary Fig. 4, related to Fig. 2

a, Violin plot showing the distributions for each sample of number of genes detected per cell.

b, Violin plot showing the distributions for each sample of number of gene expression UMIs detected per cell.

c, Violin plot showing the distributions for each sample of TSS enrichment scores per cell.

d, Violin plot showing the distributions for each sample of the fraction of ATAC fragment reads that are detected in peaks per cell.

e, Plot showing the percentage of called cells for each sample that had a single spatial location.

f, Violin plot showing the distributions for each sample of the number of spatial barcode UMIs detected per cell.

Further Slide-tags QC metrics can be found in Supplementary Table 1.

Supplementary Fig. 5

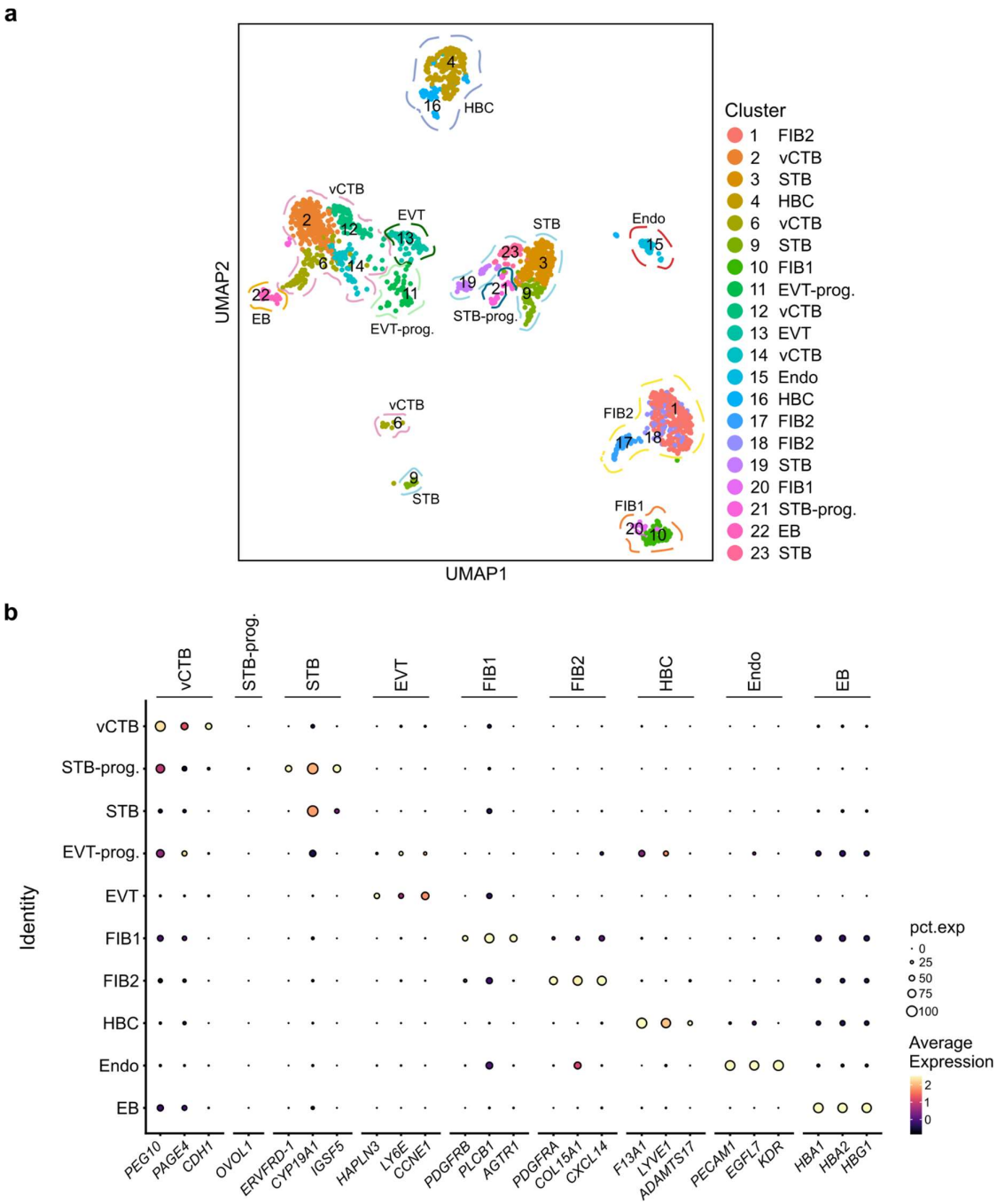

Supplementary Fig. 5, related to Fig. 2

a, UMAP plot showing clustering and corresponding cell type annotation for Slide-tags data. Cluster-specific differentially expressed marker genes from Slide-tags data can be found in Supplementary Table 6.

b, Dotplot showing average expression levels for selected canonical marker genes across clusters, which guided cluster annotation.

Supplementary Fig. 6

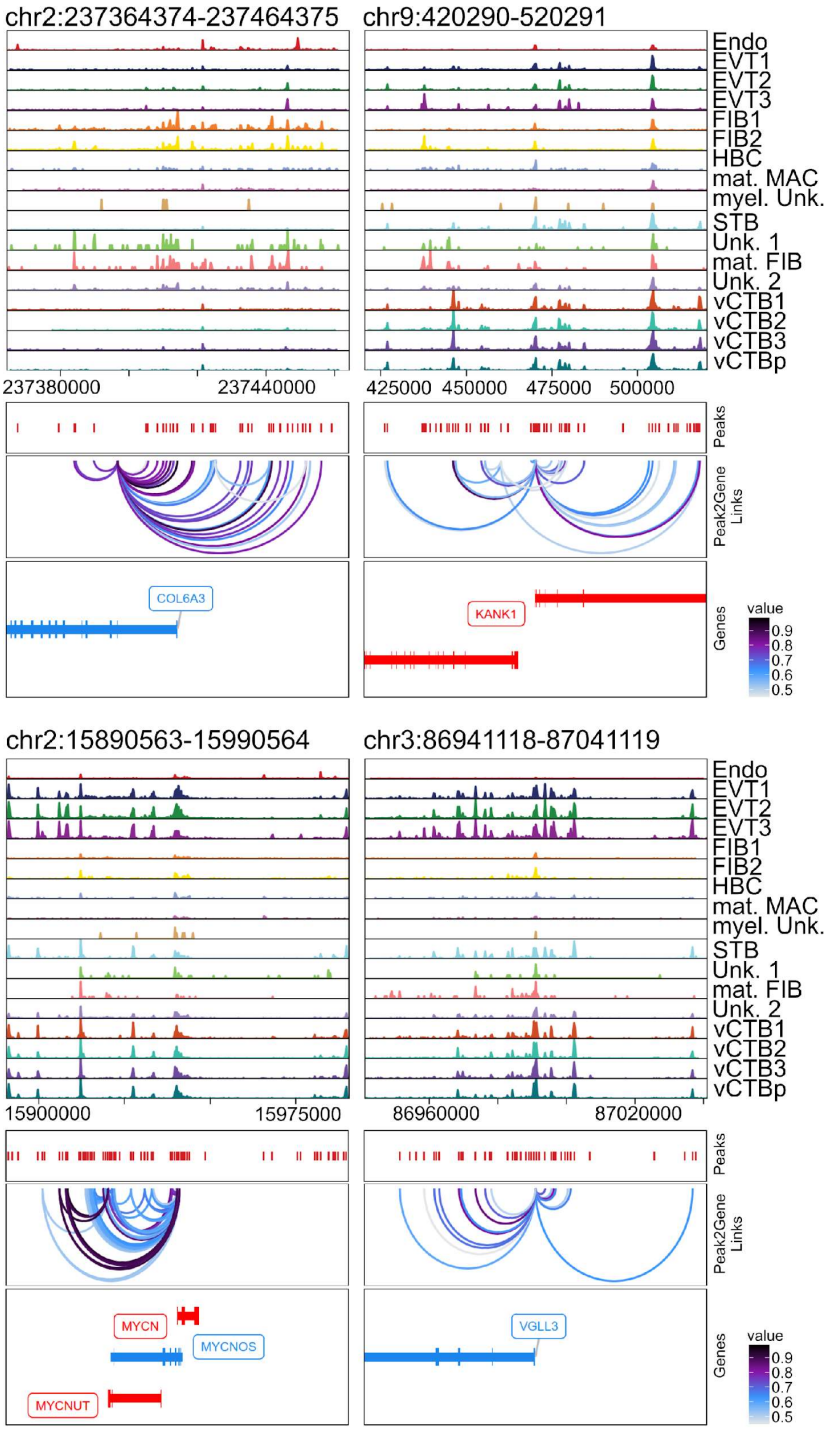

Supplementary Fig. 6, related to Fig. 3

Track visualization of *COL6A3*, *KANK1*, *MYCN/MYCNUT*, and *VGLL3*, which showed additional chromatin accessibility in: FIB1, FIB2, Unk. 1, mat. FIB (*COL6A3*); vCTB1-3, vCTBp (*KANK1*); EVT1-3 (*MYCN/MYCNUT, VGLL3*). Each track is accompanied by all significant peak-gene links identified for that gene.

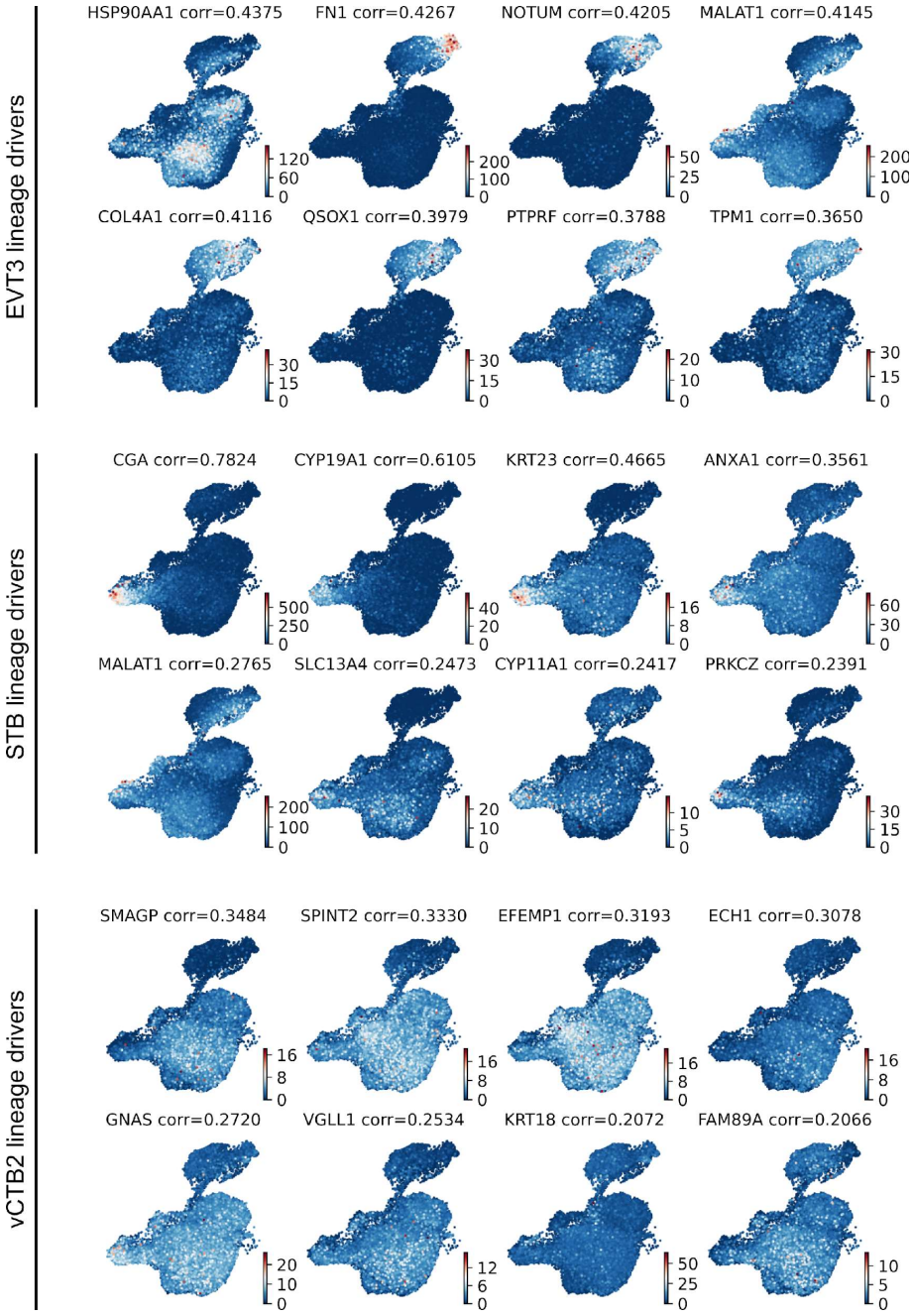

Supplementary Fig. 7, related to Fig. 3

Top lineage drivers for chromatin potential/CellRank-derived terminal states (EVT3, STB, vCTB2), calculated by finding the genes with the highest correlation (colorbar) between their expression values and transition probability (Methods). EVT3: *HSP90AA1*, *FN1*, *NOTUM*, *MALAT1*, *COL4A1*, *QSOX1*, *PRPRF*, *TPM1*. STB: *CGA, CYP19A1*, *KRT23*, *ANXA1*, *MALAT1*, *SLC13A4*, *CYP11A1*, *PRKCZ*. vCTB2: *SMAGP*, *SPINT2*, *EFEMP1*, *ECH1*, *GNAS*, *VGLL1*, *KRT18*, *FAM89A*. All lineage drivers are listed in Supplementary Table 8.

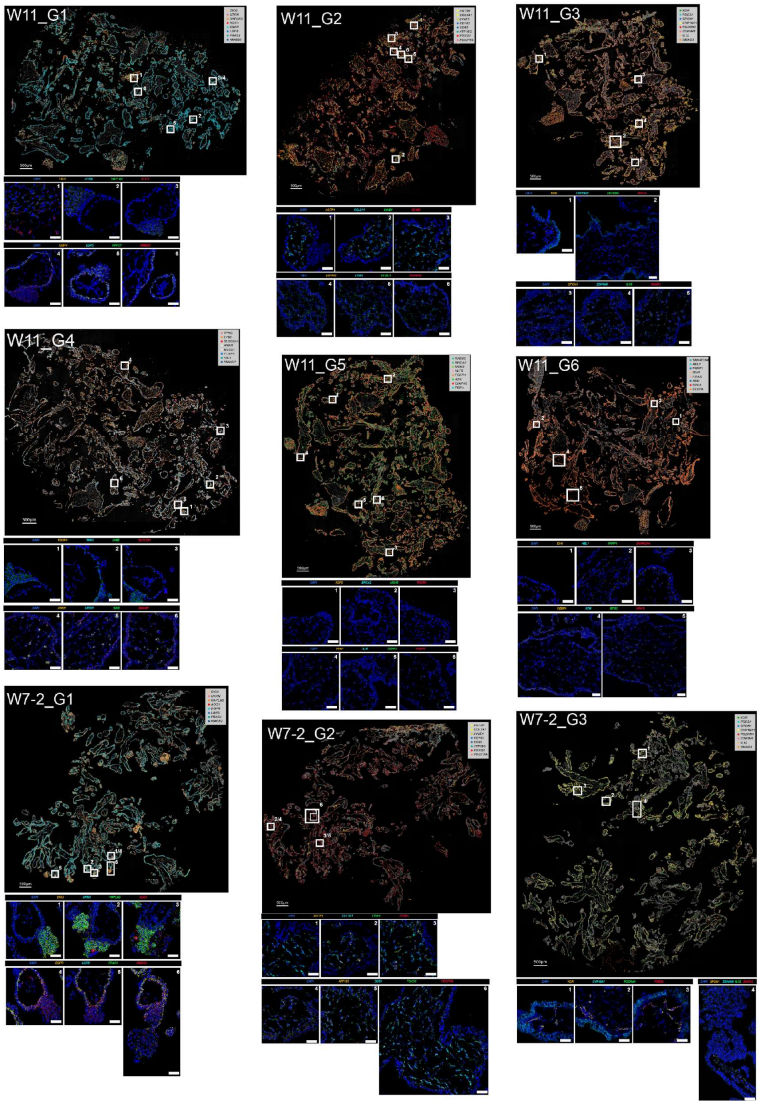

Supplementary Fig. 8: Overview of STARmap-ISH in different groups, related to Figure 4.

Global overview of the entire STARmap-ISH (n = 3) section for gene groups (G) co-detecting 8 genes per group and section, in samples W11 (G1 - G6) and W7-2 (G1 - G3). Insets depict high-resolution images of various regions across each section. G1 (*DIO2, UTRN, HAPLN3, AOC1, EGFR, LGR5, FRAS1, HMGB2*); G2 (*AGTR1, COL3A1, LYVE1, CD163, CD83, ATP1B3, FOXO1, PDGFRA*); G3 (*KDR, PDE3A, SPON1, CYP19A1, PDZRN4, ZSWIM6, IL15, SMAD3*); G4 (*TFRC, LY6E, SLCO2A1, ANKH, MTSS1, FOXP1, SIK3, SMAGP*); G5 (*RAD50, BRCA2, MSH3, KLF5, FGFR1, ATR, DIAPH2, PER1*); G6 (*SMARCA4, ABL1, PARP1, IDH1, HRAS, ATM, BTG2, CEBPA*). Scale bar = 50 µm. Genes are listed and described in Supplementary Table 11.

Supplementary Fig. 9

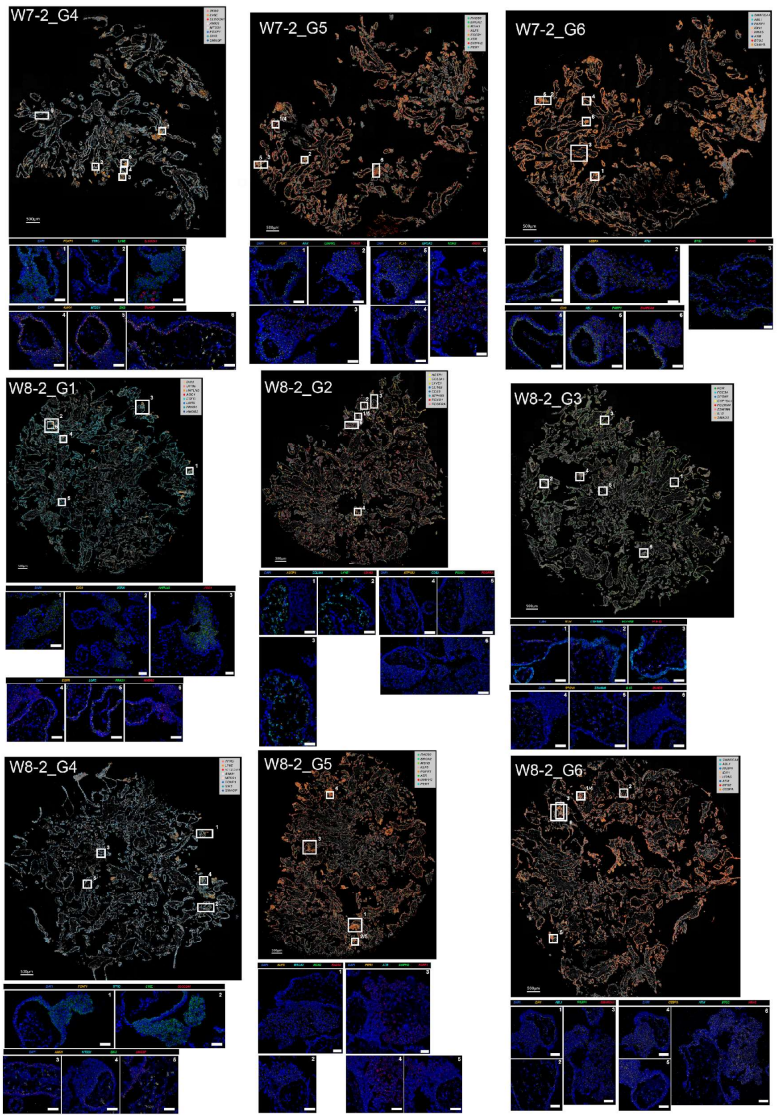

Supplementary Fig. 9: Overview of STARmap-ISH in different groups, related to Figure 4.

Global overview of the entire STARmap-ISH (n = 3) section for gene groups (G) co-detecting 8 genes per group and section, in samples W7-2 (G4 - G6) and W8-2 (G1 - G6). Insets depict high-resolution images of various regions across each section. G1 (*DIO2, UTRN, HAPLN3, AOC1, EGFR, LGR5, FRAS1, HMGB2*); G2 (*AGTR1, COL3A1, LYVE1, CD163, CD83, ATP1B3, FOXO1, PDGFRA*); G3 (*KDR, PDE3A, SPON1, CYP19A1, PDZRN4, ZSWIM6, IL15, SMAD3*); G4 (*TFRC, LY6E, SLCO2A1, ANKH, MTSS1, FOXP1, SIK3, SMAGP*); G5 (*RAD50, BRCA2, MSH3, KLF5, FGFR1, ATR, DIAPH2, PER1*); G6 (*SMARCA4, ABL1, PARP1, IDH1, HRAS, ATM, BTG2, CEBPA*). Scale bar = 50 µm. Genes are listed and described in Supplementary Table 11.

Supplementary Fig. 10

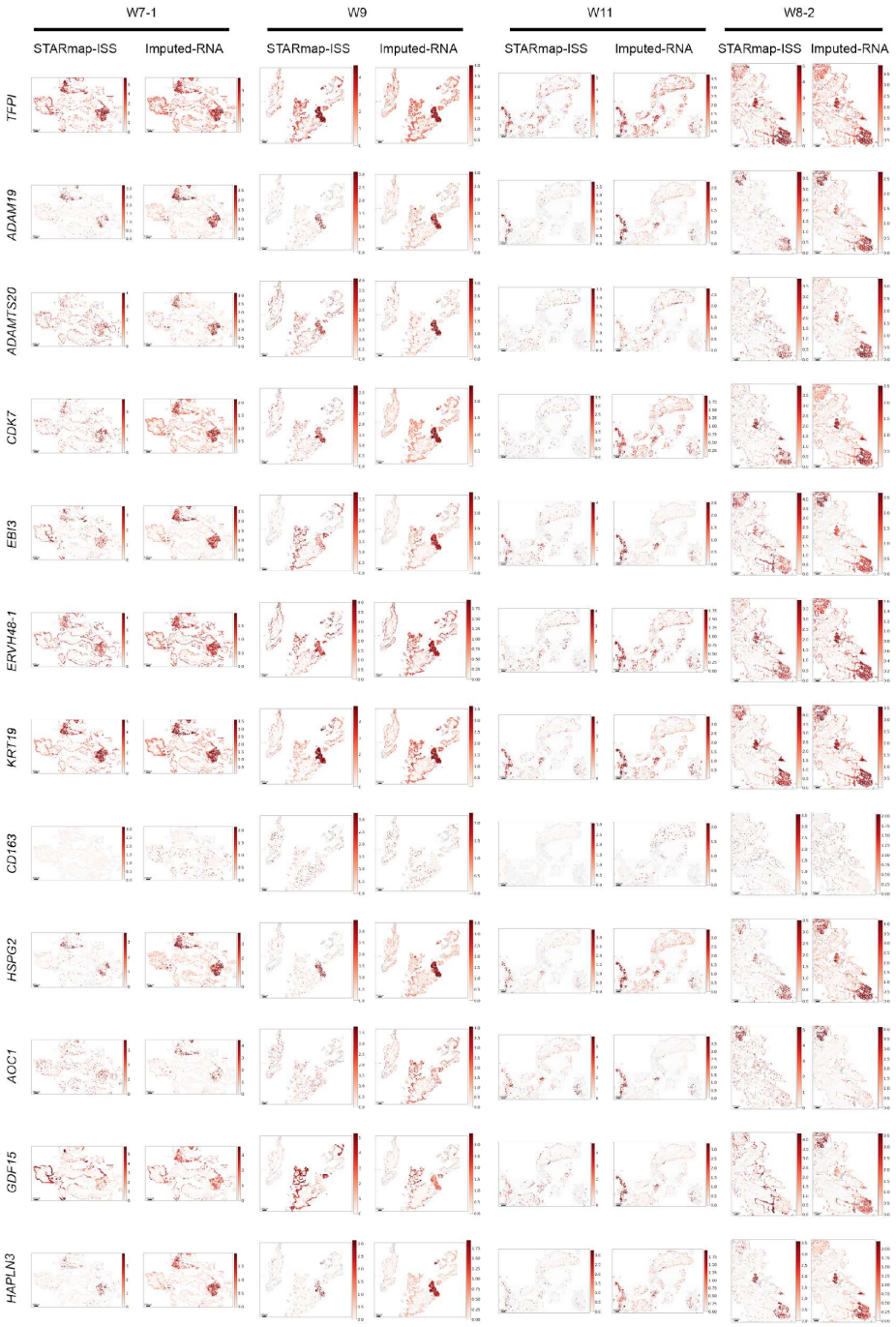

Supplementary Fig. 10: More examples of imputed spatial gene expression relative to observed expression, related to Figure 6.

STARmap-ISS (n = 4) and corresponding imputed gene expression (Imputed-RNA) across placental samples W7-1, W9, W11, and W8-2 for vCTB/EVT-enriched *ERVH48-1*, EVT-enriched genes (*TFPI, ADAM19, ADAMTS20, CDK7, HSPG2, HAPLN3, AOC1, KRT19*), HBC marker *CD163*, and STB-enriched genes (*GDF15, EBI3*).

Supplementary Fig. 11

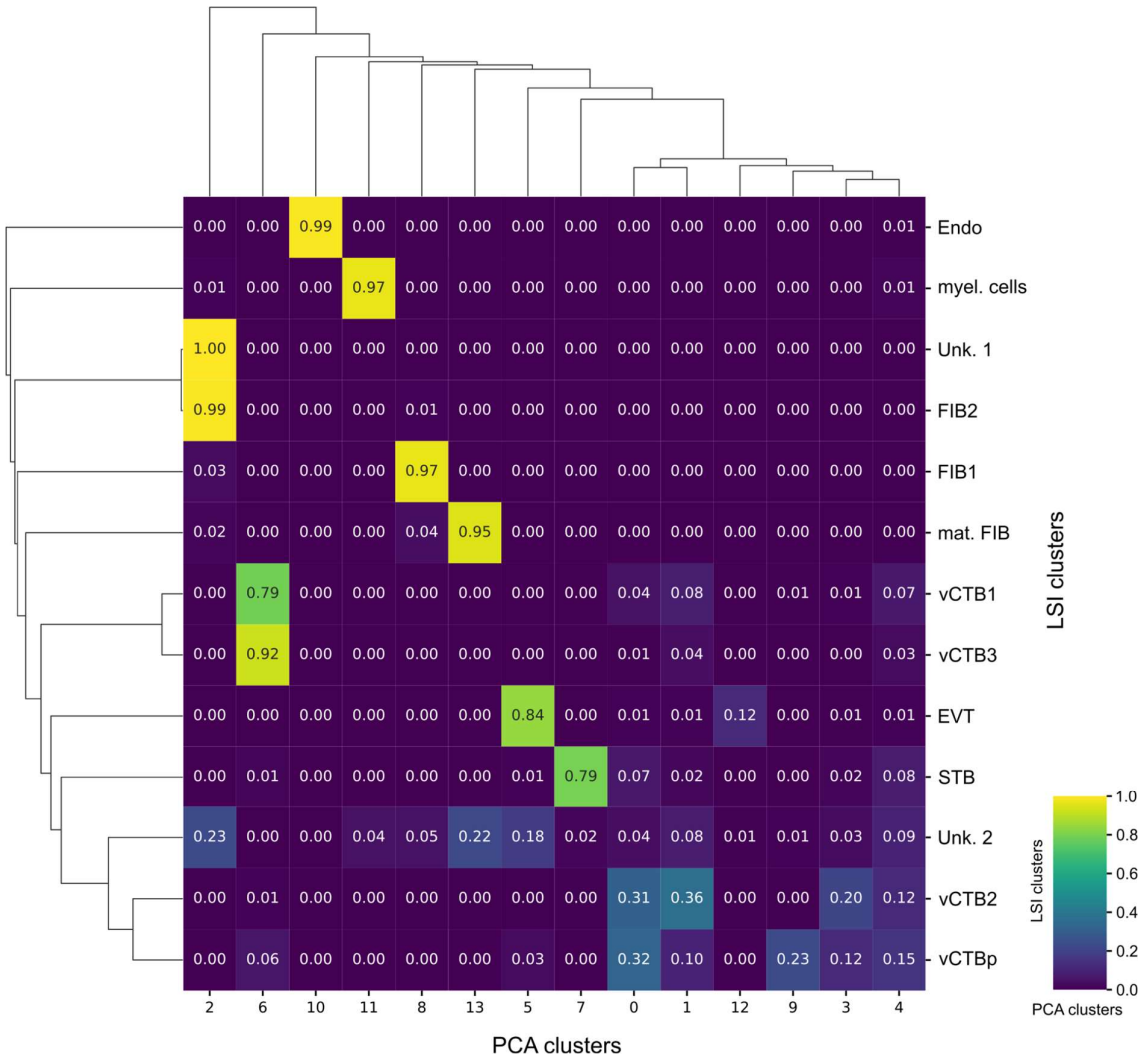

Supplementary Fig. 11: Comparative analysis of clustering using PCA vs. LSI for RNA data, related to Methods.

Confusion matrix displaying Louvain clusters, with the y-axis showing annotated clusters generated using LSI for both RNA and ATAC modalities, and the x-axis presenting clusters derived from PCA for RNA and LSI for ATAC. The color gradient and the numbers indicate the fraction of cells from each annotated LSI-LSI cluster found within the PCA-LSI clusters, highlighting significant overlap among the main cell populations.

Supplementary Table 1

Information about the human primary samples isolated from first trimester placentas and used in this study along with accompanying assays: multiome (combined snRNA-seq and snATAC-seq), Slide-tags, STARmap-ISS, and STARmap-ISH. Each assay is accompanied by relevant quality control metrics.

Supplementary Table 2

Differentially expressed genes discovered by snRNA-seq.

Supplementary Table 3

Differentially accessible genes discovered by snATAC-seq.

Supplementary Table 4

Intercluster motif enrichment comparisons. Differentially accessible peaks were identified using a two-sided Wilcoxon test (FDR ≤ 0.1, log2 fold change ≥ 0.5). Intercluster motif enrichments were calculated via a hypergeometric test to generate p-values. For instance, "vCTBvsEVT" lists motifs enriched across peaks that are more accessible in vCTB clusters compared to EVT clusters.

Supplementary Table 5

ChromVAR motif enrichment analysis and accompanying positive TF regulators. Correlation between variables (motif enrichment, gene expression, gene accessibility) was calculated using Pearson's correlation coefficient, and statistical significance was assessed using p-values adjusted by the Benjamini-Hochberg method (padj $< .01$).

Supplementary Table 6

Cluster-specific differentially expressed marker genes across all clusters identified by Slide-tags, along with spatially autocorrelated genes and TF motifs with location-dependent expression and enrichment as identified by Slide-tags analysis using Moran’s I (includes correlations across all cells as well as within individual cell types). P-values were adjusted using the Benjamini-Hochberg procedure ($p < .05$). Cluster numbering can be found in Supplementary Figure 5.

Supplementary Table 7

Inferred peak-gene links, DORCs, and per cluster DORC scores. snRNA-seq-identified tumor invasion and immunomodulation-related genes overlapped with DORCs, namely *RUNX1*, *C12orf75*, *QSOX1*, *RASGRF2*, *PLXNB2*, *JAK1*, and *MYCN*. Overlap with snATAC-seq-identified genes included *ATP11A*, *DIO2*, *ANXA1*, *KLF6*, *ASCL2*, *NR2F6*, *SNAI2*, *TCF21*, *FLI1*, *PITX1*, *GRHL1*, and *NFIX*.

Supplementary Table 8

Lineage drivers for chromatin potential/CellRank-derived terminal states (EVT3, STB, vCTB2) calculated by CellRank analyses. P-values of the two-sided Fisher transformation tests were calculated and adjusted using Storey-Tibshirani procedure for multiple hypothesis comparisons.

Supplementary Table 9

Description of UKBB pregnancy-related traits and accompanying heritability enrichments across cell types.

Supplementary Table 10

MAGMA gene set enrichment analysis of cell type-specific programs for each cell type as well as enrichment analysis of top GWAS hits for each pregnancy-related trait across cell types.

Supplementary Table 11

1,001 genes for STARmap-ISS and 48 genes for STARmap-ISH and accompanying probe sequences used for *in situ* sequencing and *in situ* hybridization.

Supplementary Table 12

Differentially expressed genes identified by STARmap-ISS. Statistics were derived using wilcoxon test (two-sided). P-values were adjusted using the Benjamini-Hochberg method.

Supplementary Table 13

Ligand-receptor interactions across clusters and samples. Interaction (communication) probabilities and significance were computed by permutation test ($p < .05$).

References

1. Muralimanoharan, S., Guo, C., Myatt, L. & Maloyan, A. Sexual dimorphism in miR-210 expression and mitochondrial dysfunction in the placenta with maternal obesity. *Int. J. Obes.* **39**, 1274–1281 (2015).
2. Huang, J., Chen, W., Jie, Z. & Jiang, M. Comprehensive Analysis of Immune Implications and Prognostic Value of SPI1 in Gastric Cancer. *Front. Oncol.* **12**, 820568 (2022).
3. Villar, J. *et al.* ETV3 and ETV6 enable monocyte differentiation into dendritic cells by repressing macrophage fate commitment. *Nat. Immunol.* **24**, 84–95 (2023).
4. Yang, M.-G. *et al.* Biological characteristics of transcription factor RelB in different immune cell types: implications for the treatment of multiple sclerosis. *Mol. Brain* **12**, 115 (2019).
5. Eluard, B. *et al.* The alternative RelB NF-κB subunit is a novel critical player in diffuse large B-cell lymphoma. *Blood* **139**, 384–398 (2022).
6. Zhang, Z., Wang, X., Wang, J. & Zhang, L. The decreased expression of Stat3 and p-Stat3 in preeclampsia-like rat placenta. *J. Mol. Histol.* **49**, 175–183 (2018).
7. Ao, X., Ding, W., Zhang, Y., Ding, D. & Liu, Y. TCF21: a critical transcription factor in health and cancer. *J. Mol. Med.* **98**, 1055–1068 (2020).
8. Liu, D. X. & Lobie, P. E. Transcriptional activation of p53 by Pitx1. *Cell Death Differ.* **14**, 1893–1907 (2007).